A SIMULTANEOUS PHYSICAL AND SPECTRAL ANALYSIS OF THE TURBULENT BOUNDARY LAYER VIA TIME-RESOLVED PARTICLE IMAGE VELOCIMETRY

Jeffrey A. LeHew
Graduate Aerospace Laboratories
California Institute of Technology
1200 E. California Blvd, MC 205-45
Pasadena, California 91125
lehew@caltech.edu

Michele Guala*
Department of Civil Engineering
University of Minnesota, Twin Cities
500 Pillsbury Dr. SE
Minneapolis, Minnesota 55455
mguala@umn.edu

Beverley J. McKeon
Graduate Aerospace Laboratories
California Institute of Technology
1200 E. California Blvd, MC 301-46
Pasadena, California 91125
mckeon@caltech.edu

ABSTRACT

In this study, time-resolved particle image velocimetry (PIV) was performed in wall-parallel planes to investigate both the time evolution of structures in the flow as well as the 3D spatio-temporal spectrum. In particular vortex signatures in wall-parallel planes were studied which were found to correspond closely with the signature of hairpin vortices found in wall-bounded shear flows. Considering the convection velocity of different streamwise-spanwise scale pairs calculated from the spatio-temporal spectrum, it was found that the average convection velocity of highly energetic scales in the range $1.5 < \lambda_x/\delta < 5.0$ and $0.5 < \lambda_z/\delta < 1.0$ was close to the convection velocity of the vortex signatures. Also, this range of wavelengths is similar in size to the streamwise-elongated structures around which these vortices often appear.

INTRODUCTION

The structure of wall-bounded shear flows has been investigated over several decades by means of statistical analysis and through the study of coherent structures, both of which have provided a basis for the development of modern flow control strategies, yet the connection between coherent structures and the energetic scales identified by statistical methods is still unclear. To help elucidate this connection, time-resolved PIV was performed in wall parallel planes to provide access to spectral information in all directions (streamwise wavenumber, spanwise wavenumber, and frequency) as well as snapshots of turbulent structures as they evolve in time.

One of the few time-resolved PIV investigations of the turbulent boundary layer was performed by Dennis & Nickels (2008) where the validity of Taylor's hypothesis was tested at $y/\delta = 0.16$ with a $6\delta \times 3\delta$ field of view, where δ is the boundary layer thickness and y is the wall-normal direction. It was shown that the long meandering structures found in the log-layer (Hutchins & Marusic, 2007), often referred to as superstructures or very large scale motions (VLSMs), appear nearly identical in the spatial and Taylor-reconstructed fields. The signature of these large scales in turbulent spectra have been shown to contain a significant portion of the turbulent kinetic energy; Balakumar & Adrian (2007) showed that streamwise scales longer than 3δ contained at least 45% of the turbulent kinetic energy in boundary layer flows. In addition, Ganapathisubramani *et al.* (2003) found that hairpin packets of comparable streamwise extent contained a significant amount of Reynolds stress, $-\overline{uv}$, and thus may be associated with significant turbulence production. In order to capture these large scale dynamics which contribute significant energy to the flow, current experiments were performed with a field of view up to 10δ in streamwise extent.

In the current study comparisons are drawn between the spectral and structural representations of the flow by considering the convection velocity of the structures in the flow as well as the convection velocity of individual scales investigated via the 3D spatio-temporal streamwise velocity spectrum.

From previous work, the heads of hairpin vortices were shown to convect near the local mean (with some deviations toward slower velocity in the wake region) by Adrian *et al.* (2000). Wu & Christensen (2006) showed similar results noting that the spread in convection velocities increased as the wall is approached and is proportional to the local RMS streamwise velocity fluctuations. In the current study, the con-

*Current address; previously at the Graduate Aerospace Laboratories at the California Institute of Technology

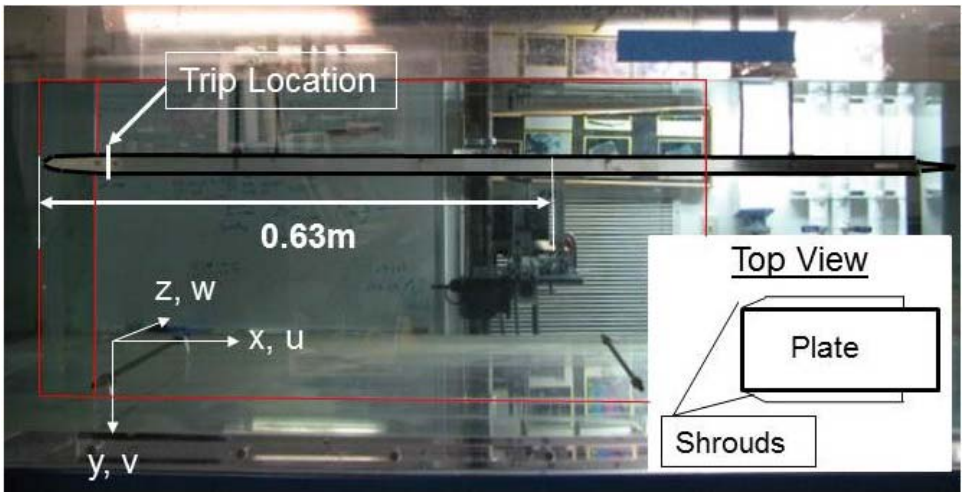

Figure 1: Test section with the submerged portion of the shroud in red. The inset provides an overhead view.

Table 1: Experimental parameters are presented with the SF parameters in parentheses where applicable.

Re_θ	δ	θ	U_∞	u_τ	ν/u_τ
1085	13.5mm	1.6mm	0.63m/s	0.028m/s	$32.9\mu m$
y^+	y/δ	U^+	Δx^+, Δz^+	L_x/δ	L_z/δ
33	0.08	14.4 (14.0)	33 (15)	10.0 (4.3)	5.0 (2.2)
58	0.14	15.0 (15.2)	34 (15)	10.2 (4.3)	5.0 (2.2)
122	0.30	16.9 (17.0)	33 (15)	10.0 (4.4)	4.9 (2.2)
198	0.48	19.0 (19.0)	32 (14)	9.5 (4.3)	4.8 (2.1)

vection velocity of the signature of these hairpin vortices in wall parallel planes is investigated. Concerning the convection velocity of scales ascertained via statistical analyses, it has been found that large streamwise scales convect faster than the local mean near the wall (Morrison *et al.*, 1971; Kim & Hussain, 1993; Krogstad *et al.*, 1998) and slower than the local mean far from the wall (Chung & McKeon, 2010; LeHew *et al.*, 2010), therefore, the behavior in both of these regions will be studied. Scale-based convection velocities from the data set presented here are compared to those of the hairpin vortex signatures which often form into streamwise elongated packet-type structures.

The experimental setup is presented first and followed by a discussion of the vortex tracking algorithm and the convection velocities measured. The spectral measurements and the convection velocity of individual scales are then presented. Finally, a comparison is made between the convection velocity of large energetic scales and the vortices observed in the flow.

EXPERIMENTAL SETUP

Measurements of a zero-pressure gradient boundary layer at $Re_\tau = \delta u_\tau/\nu = 410$ ($Re_\theta = \theta U_\infty/\nu = 1085$) were performed on a 1.1m long by 0.45m wide flat plate in a free surface water tunnel facility. $u_\tau = \sqrt{\tau_w/\rho}$ is the friction velocity, τ_w is the shear stress at the wall, ρ is the density, ν is the kinematic viscosity, U_∞ is the free-stream velocity, and θ is the momentum thickness. The 13.5mm thick boundary layer on the bottom of the plate was studied to avoid interaction with surface waves. A shroud with a wedge-shaped leading edge was placed along the sides of the plate to promote a two-dimensional flow producing a streamwise velocity variation of less than 1% of the local mean along the spanwise direction. Measurement planes were centered 0.63m downstream of the leading edge with $U_\infty = 0.63m/s$ and the free stream turbulence level less than 0.1%. A photograph showing the test section and coordinate system is presented in Fig. 1.

2D planar PIV measurements were performed in the wall-normal and wall-parallel planes in two separate sets of experiments. In both, two cameras were placed side-by-side to provide a longer field of view in the streamwise direction. For measurements in the wall-normal plane, the field of view was $5\delta \times 1.2\delta$. For measurements in the wall-parallel planes, both a large field of view (LF), $10\delta \times 5\delta$, and a small field of view (SF), $4.3\delta \times 2.2\delta$, were used to study the largest scales and resolve the smallest scales, respectively. The wall-parallel measurements were performed at 4 different wall-normal locations listed in Table 1. Images were recorded at 2500fps for the SF, 1000fps for the 3 near wall planes of the LF, and

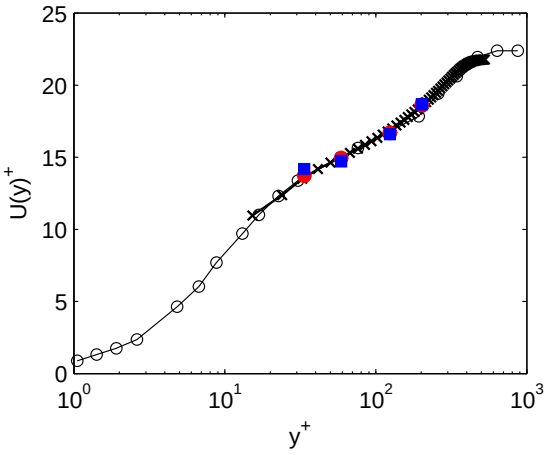

(a) Mean profile

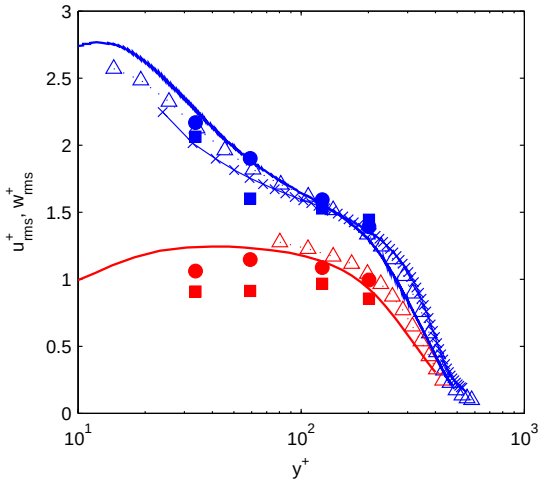

(b) RMS velocity fluctuations

Figure 2: In (a): the mean velocity profile is presented where the symbols are –x–: Mean profile from wall-normal measurements, –o–: data from DeGraaff & Eaton (2000) at Re_θ = 1430, •: mean velocity from wall-parallel SF measurements, ▪: mean velocity from wall-parallel LF measurements. In (b): the rms velocity fluctuations are presented where the symbols are –x–: u^+_{rms} from the wall normal measurements, •: wall-parallel SF measurements, ▪: wall-parallel LF measurements, – – △ – –: data from Erm & Joubert (1991) at Re_θ = 1003, —: data from Wu & Moin (2009) at Re_θ = 900.

1500fps for the LF at y^+ = 198 giving Δt^+ = 0.34, 0.86, and 0.57, respectively. See LeHew *et al.* (2011) for more details on the experimental setup and PIV system.

The mean velocity profile is presented in Fig. 2a and the rms velocity fluctuations from both wall-normal and wall-parallel planes are shown in Fig. 2b and agree well with the literature. The underestimation of w^+_{rms} using the LF data is expected and explained by LeHew *et al.* (2011). For this reason, any analysis requiring a spanwise velocity is only investigated using the SF data. To calculate u_τ, a least squares fit to the predetermined log layer was performed and δ was defined

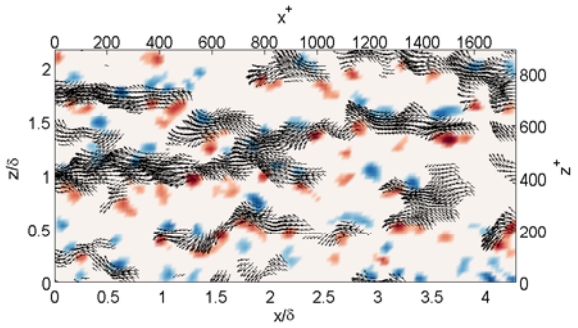

Figure 3: At y^+ = 58, vortices with CW (blue) and CCW (red) rotation are shown amongst low momentum regions indicated by the velocity vectors.

using the $U(y) = 0.99U_\infty$ criterion. The key parameters for the wall parallel measurements are recorded in Table 1.

VORTEX TRACKING

The main structures investigated in this study were vortices in wall-parallel planes which were found to closely match the signature of hairpin vortex structures. To identify these vortices, the swirling strength field was first calculated using Eq. 1, where $\lambda_{c,i}$ is the swirling strength and u and w are the fluctuating velocities in the streamwise, x, and spanwise, z, directions, respectively. The swirling strength is the imaginary part of the complex eigenvalue of the local velocity-gradient tensor and is useful for revealing regions of rotational flow as discussed by Zhou *et al.* (1999). Individual cores are identified using using a threshold of $|\lambda_{c,i}| \geq 1.5(\lambda_{c,i})_{rms}$, which was also used by Wu & Christensen (2006) and found to be an appropriate cutoff. To ascertain the direction of the swirling motion, the signed swirling strength, $\Lambda_{c,i}$, is used as given in Eq. 2, where ω_y is the local out-of-plane vorticity.

$$\lambda_{c,i} = \left| Im\left[\sqrt{\left(\frac{\partial u}{\partial x} + \frac{\partial w}{\partial z}\right)^2 + 4\left(\frac{\partial u}{\partial x}\frac{\partial w}{\partial z} - \frac{\partial u}{\partial z}\frac{\partial w}{\partial z}\right)} \right] \right| \quad (1)$$

$$\Lambda_{c,i} = \|\lambda_{c,i}\| \frac{\omega_y}{\|\omega_y\|} \quad (2)$$

Vortices in wall parallel planes were found to exist near the interface of high and low momentum regions, defined as regions in which the local velocity is 10% higher and 10% lower than the mean velocity in the plane of interest, respectively. A representative snapshot of vortices amongst low momentum regions is shown in Fig.3, where pairs of opposite signed vortices are found to flank these low momentum regions.

To identify whether these swirling regions are representative of hairpin vortices, their average shape was studied by finding the distribution of their equivalent diameters, D_{eq},

($D_{eq} = \sqrt{4A/\pi}$, where A is the area of the vortex) and eccentricity, ε, (For an ellipse, $\varepsilon = \sqrt{1-(b/a)^2}$, where a and b are the major and minor axes, respectively). From the well-resolved SF data, it was found that $D^+_{eq} \approx 54$ on average where the distribution of sizes increases moving away from the wall. For all planes, $\varepsilon \approx 0.75$ in the mean with a distribution between 0.5 and 0.9, where planes further from the wall favor smaller values of ε, i.e. more circular shapes. A streamwise elongated shape is expected for a hairpin vortex (Tomkins & Adrian, 2003) due to their tilting with respect to the streamwise direction which tends to be at an angle of 45^o on average (Head & Bandyopadhyay, 1981). A circular vortex tube tilted at 45^o would produce $\varepsilon = 1/\sqrt{2} \approx 0.71$, which matches well with the ε found from the present data. Also, the decrease in ε further from the wall may be indicative of the reduced inclination of the vortex as it approaches the free-stream (See Ganapathisubramani *et al.* (2006)). Altogether, the vortex signatures identified seem to be hairpin vortices.

To track vortices in time, a weighted centroid is used to identify the position of each vortex at each time step. For each frame, the algorithm looks for the nearest neighbor under the constraint that the vortex move in the streamwise direction no faster than the U_∞ (with a ± 1 vector displacement error to account for inaccuracies in finding the centroid). In all cases over 50% of all swirling regions identified were tracked in time. Of those, 10-30% persisted for at least one eddy turnover time ($T_E = \delta/U_\infty$). The pdfs of the vortex convection velocities for each wall-parallel plane are shown in Fig. 4 for vortices that persisted for T_E or longer. The axes extend from $u^+ = 10$, the minimal convection velocity in the flow, to $u^+ = 22$, the free-stream velocity, in which almost all of the tracked vortices fall. These pdfs show a large spread of convection velocities likely indicating a large spread in vortex heights as hairpin vortex heads were found to travel at the local mean velocity by Wu & Christensen (2006). It appears that, on average, vortices tend to convect slower than the local mean, particularly for planes far from the wall. The difference between the LF and SF data is only very noticable at $y^+ = 33$ with the LF data indicating that vortices convect close to the local mean, while the SF data indicates much slower convection velocities. Having vortex convection velocities slower than the local mean in all cases would indicate that the heads of these hairpins, which exist further from the wall, should also travel slower than the local mean, which is in contrast to other measurements in the literature (Adrian *et al.*, 2000; Wu & Christensen, 2006). A study of the time-evolution of wall-normal structures would be of interest to investigate this point.

Next, convection velocities of different scales in the flow are studied using the 3D spatio-temporal streamwise velocity spectrum.

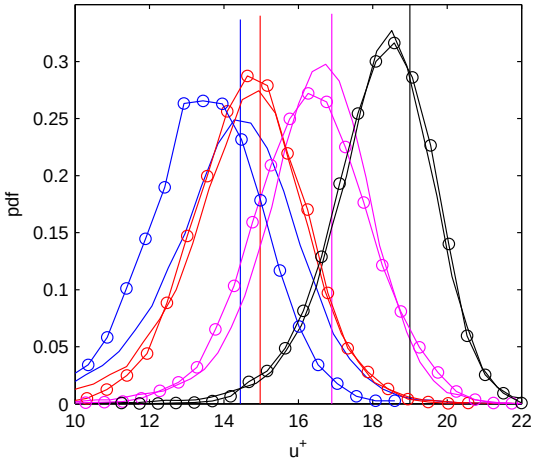

Figure 4: A pdf of vortex convection velocities is shown for vortices that persist for $T_E = \delta/U_\infty$ or longer for both the LF (—) and SF (–o–) data. The mean velocity for each plane of the LF data is shown by the vertical line where the colors represent different wall normal locations; blue: $y^+ = 33$, red: $y^+ = 58$, magenta: $y^+ = 122$, black: $y^+ = 198$.

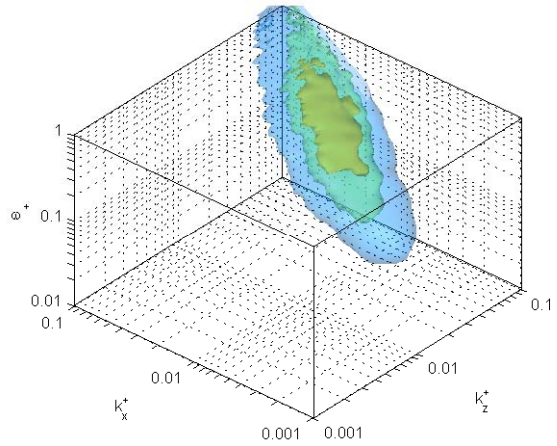

Figure 5: $k_x k_z \omega \Theta(k_x, k_z, \omega)$ is presented at $y^+ = 58$ using the SF data. The surfaces represent 25%, 50%, and 75% of the total energy in the spectrum moving from blue to yellow. The shape of the spectrum is qualitatively similar in the other planes

SPECTRAL ANALYSIS

The 3D spatio-temporal streamwise velocity spectrum (2D in space, 1D in time) is calculated as described by LeHew *et al.* (2011). The spectrum at $y^+ = 58$ is shown in Fig. 5 where k_x, k_z, and ω are the streamwise wavenumber, spanwise wavenumber, and angular frequency, respectively.

This spectrum can be thought of as a decomposition of the data into a number of streamwise-spanwise scale pairs that convect downstream at a speed equal to $u_{c,x} = \omega/k_x$, where a range of convection velocities exists for each scale pair. The spectrum shows the amplitude of each of these traveling waves and can be used to identify the dominant ones. A single representative convection velocity can be calculated for each streamwise-spanwise scale pair using Eq. 3 from del Álamo & Jiménez (2009) and used in earlier works by Jiménez *et al.* (2004) and Flores & Jiménez (2006).

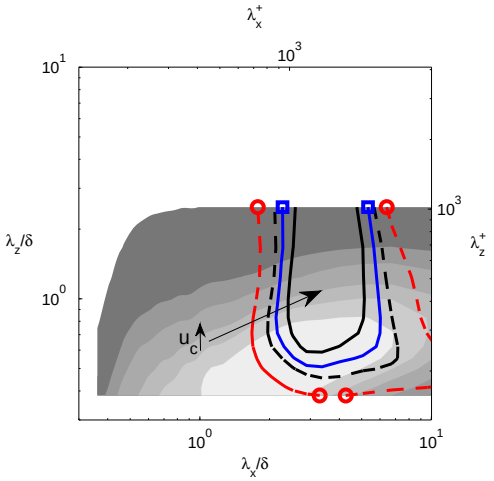

Figure 6: The contour lines represent u_c at $y^+ = 33$ calculated using Eq. 3 with the LF data. The black contours lines are u_c equal to the local mean for the LF (solid) and the SF (dashed), the blue line is u_c equal to the mean vortex convection velocity for the LF ($u^+ = 14.2$) and the red is for the SF ($u^+ = 13.5$). The arrow indicates the direction of increasing u_c. The shaded contours represent 20 to 80% of the maximum energy of $k_x k_z \Phi(k_x, k_z)$ in 10% increments moving from light to dark shades.

$$u_c(k_x, k_z, y) = \frac{1}{k_x} \frac{\int_{-\infty}^{\infty} \omega \Theta(k_x, k_z, \omega, y) d\omega}{\int_{-\infty}^{\infty} \Theta(k_x, k_z, \omega, y) d\omega} \qquad (3)$$

This method provides a measure of the convection velocity where the ω in ω/k_x is weighted by the 3D spectrum, or in other words, this method picks a dominant frequency based on the "center of mass" of the spectrum in ω. A map of this convection velocity measure is plotted on top of the 2D pre-multiplied streamwise velocity spectrum $k_x k_z \Phi(k_x, k_z)$ in Fig. 6, where the spectrum helps to highlight the range of convection velocities for the most energetic scales in the flow.

From Fig. 6 it is apparent that scales in the range $2.5 < \lambda_x/\delta < 5$ and $\lambda_z/\delta > 0.6$ (equivalently $1000 < \lambda_x^+ < 2000$ and $\lambda_z^+ > 250$) move faster than the local mean velocity while the convection velocity is slower elsewhere in this plane, where λ_x and λ_z are the streamwise and spanwise wavelength, respectively. Since this map is shown only for the LF data, it is likely that convection velocities for the smaller wavelengths are underestimated (due to a limited range of ω for the LF spectrum), but the focus here is on the large scales which are correctly resolved in the current data set. In subsequent planes, the region where convection velocities are greater than the local mean shrinks and eventually, most scales tend to convect slower than the local mean. The contours of u_c equal to the vortex convection velocity, also shown in Fig. 6, tend to move toward shorter streamwise wavelengths as the free-stream is approached but also extend over larger ranges of z. At $y^+ = 33$, the convection velocity contours roughly cuts a rectangular region with edges at $\lambda_x/\delta = 2$ and 6, while at $y^+ = 198$, the region is bounded by $\lambda_x/\delta = 0.6$ and 1.9. In all planes, these contours cut through regions which contain the most energetic scales in the flow as documented in Table 2.

Table 2: Left columns: Scales traveling at the mean vortex convection velocity, Right columns: Most energetic range of scales used for spectral convection velocities in Fig. 7

y^+	λ_x/δ	λ_z/δ	λ_x/δ	λ_z/δ
33	2.0, 6.0	0.5-2.5	1.4-5.1	0.4-0.7
58	1.2, 5.5	0.7-2.5	1.5-5.2	0.5-0.8
122	0.7, 4.5	0.4-2.5	1.5-5.0	0.6-1.0
198	0.6, 1.9	0.4-2.5	1.5-3.8	0.6-1.2

To close the loop, we compare the vortex convection velocities to the average convection velocities of the scales that contain the top 10% of the energy (i.e. the white region in Fig. 6). The range of scales investigated is documented in Table 2 for each wall-normal location. The comparison between these convection velocities and the vortex convection velocities is shown in Fig. 7. The error bars in Fig. 7 illustrate the width of the vortex convection velocity pdfs and they denote data within 2 standard deviations of the mean. There is a close correspondence between the convection velocities of these energetic scales and the convection velocity of the vortices in the flow. The range of scales chosen for comparison was relevant since in each plane investigated, the convection velocity in part of this region was always equal to the vortex convetion velocity. It is notable that the mean convection velocity of the vortices investigated here which were of size $\lambda_x^+ = 50$ ($\lambda_x/\delta \approx 0.1$) is equivalent to that of scales that are generally on the order of δ in streamwise extent. Considering that hairpin vortices tend to aggregate into packets that extend up to streamwise lengths of 3δ and larger (Ganapathisubramani *et al.*, 2003), it is likely that these energetic regions are related to hairpin packets. In addition, by using the range of streamwise scales listed in Table 2 and filtering the original velocity fields in x we retain the large low-momentum regions and the pattern of opposite signed swirl flanking these regions as shown in Fig. 8, which can be compared to the original field in Fig. 3. This connection shows promise for finding further, more detailed connections between energetic structures in the flow and energetic scales identified by spectral analysis.

CONCLUSIONS

Using time-resolved PIV and resolving scales from $\lambda_x^+ = 30$ to $\lambda_x/\delta = 10$, both the evolution of coherent structures in the flow, with a focus on the convection of vortices in the flow, and the 3D spatio-temporal spectrum were studied. A close relationship between the vortex convection velocity and the convection velocity of a range of energetic large scales was found. From a further analysis, it may be possible to find other connections between coherent structures in the flow and traveling waves over a particular range of sizes and speeds.

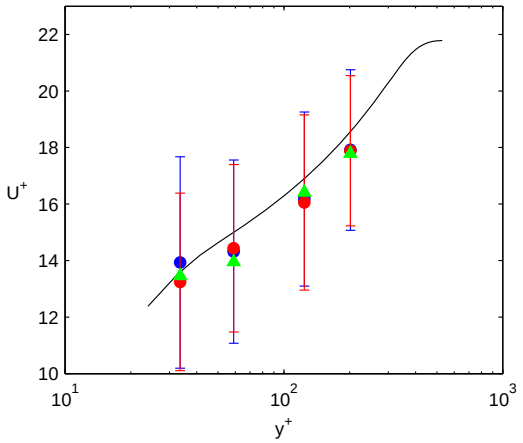

Figure 7: The convection velocity of vortices are shown for each plane with the red (SF) and blue (LF) data points. The error bars indicate 2 standard deviations covering nearly the entire range of the pdfs in Fig.4. The green triangles indicate the mean convection velocity of the most energetic scales in the flow containing 10% of the total energy.

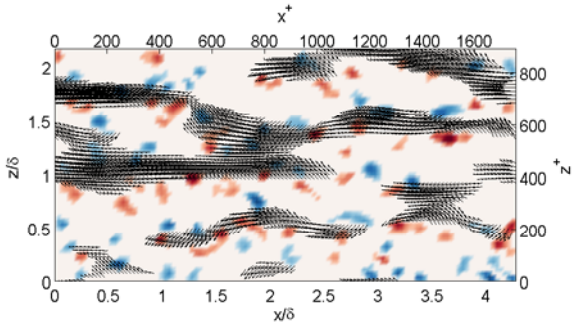

Figure 8: Same as Fig. 3 except a spatial band-pass filter has been applied to the velocity field (not the swirl field) to only allow the range $1.3 < \lambda_x/\delta < \infty$, where the difference in the filtered wavelengths from Table 2 is due to the difference in the resolution between the LF and SF data sets.

ACKNOWLEDGEMENTS

We would like to thank the Air Force Office of Scientific Research for their support of this research under award number #FA9550-09-1-0701.

REFERENCES

Adrian, R. J., Meinhart, C. D. & Tomkins, C. D. 2000 Vortex organization in the outer region of the turbulent boundary layer. *J. Fluid Mech.* **422**, 1–54.

Balakumar, B. J. & Adrian, R. J. 2007 Large- and very-large-scale motions in channel and boundary-layer flows. *Phil. Trans. Royal Soc. A* **365**, 665–681.

Chung, D. & McKeon, B. J. 2010 Large-eddy simulation of large-scale structures in long channel flow. *J. Fluid Mech.* **661**, 341–364.

DeGraaff, D. B. & Eaton, J. K. 2000 Reynolds-number scaling of the flat-plate turbulent boundary layer. *J. Fluid Mech* **422**, 319–346.

del Álamo, J. C. & Jiménez, J. 2009 Estimation of turbulent convection velocities and corrections to Taylor's approximation. *J. Fluid Mech.* **640**, 5–26.

Dennis, D. J. C. & Nickels, T. B. 2008 On the limitations of Taylor's hypothesis in constructing long structures in a turbulent boundary layer. *J. Fluid Mech.* **614**, 197–206.

Erm, L. P. & Joubert, P. N. 1991 Low-Reynolds-number turbulent boundary layers. *J. Fluid Mech.* **230**, 1–44.

Flores, O. & Jiménez, J. 2006 Effect of wall-boundary disturbances on turbulent channel flows. *J. Fluid Mech.* **566**, 357–376.

Ganapathisubramani, B., Longmire, E. K. & Marusic, I. 2003 Characteristics of vortex packets in turbulent boundary layers. *J. Fluid Mech.* **478**, 35–46.

Ganapathisubramani, B., Longmire, E. K. & Marusic, I. 2006 Experimental investigation of vortex properties in a turbulent boundary layer. *Phys. Fluids* **18**.

Head, M. R. & Bandyopadhyay, P. 1981 New aspects of turbulent boundary-layer structure. *J. Fluid Mech.* **107**, 297–338.

Hutchins, N. & Marusic, I. 2007 Evidence of very long meandering features in the logarithmic region of turbulent boundary layers. *J. Fluid Mech.* **579**, 1–28.

Jiménez, J., del Álamo, J. C. & Flores, O. 2004 The large-scale dynamics of near-wall turbulence. *J. Fluid Mech.* **505**, 179–199.

Kim, J. & Hussain, F. 1993 Propagation velocity of perturbations in turbulent channel flow. *Phys. Fluids A* **5** (3), 695–706.

Krogstad, P. A., Kaspersen, J. H. & Rimestad, S. 1998 Convection velocities in a turbulent boundary layer. *Phys. Fluids* **10** (4), 949–957.

LeHew, J., Guala, M. & McKeon, B. J. 2010 A study of convection velocities in a zero pressure gradient turbulent boundary layer. *AIAA-2010-4474* .

LeHew, J., Guala, M. & McKeon, B. J. 2011 A study of the three-dimensional spectral energy distribution in a zero pressure gradient turbulent boundary layer. *Exp. Fluids* (Accepted).

Morrison, W. R. B., Bullock, K. J. & Kronauer, R. E. 1971 Experimental evidence of waves in the sublayer. *J. Fluid Mech.* **47**, 639–656.

Tomkins, C. D. & Adrian, R. J. 2003 Spanwise structure and scale growth in turbulent boundary layers. *J. Fluid Mech.* **490**, 37–74.

Wu, X. & Moin, P. 2009 Direct numerical simulation of turbulence in a nominally zero-pressure-gradient flat-plate boundary layer. *J. Fluid Mech.* **630**, 5–41.

Wu, Y. & Christensen, K. T. 2006 Population trends of spanwise vortices in wall turbulence. *J. Fluid Mech.* **568**, 55–76.

Zhou, J., Adrian, R. J., Balachandar, S. & Kendall, T. M. 1999 Mechanisms for generating coherent packets of haripin vortices in channel flow. *J. Fluid Mech.* **387**, 353–396.